Available online at www.sciencedirect.com
SCIENCE DIRECT®
Advances in Space Research 33 (2004) 1938–1944
ADVANCES IN SPACE RESEARCH (a COSPAR publication)
www.elsevier.com/locate/asr

MGS MAG/ER observations at the magnetic pileup boundary of Mars: draping enhancement and low frequency waves

C. Bertucci [a,*], C. Mazelle [a], D.H. Crider [b], D.L. Mitchell [c], K. Sauer [d], M.H. Acuña [b], J.E.P. Connerney [b], R.P. Lin [c], N.F. Ness [e], D. Winterhalter [f]

[a] CESR-CNRS/UPS, 9 Avenue du Colonel Roche, 31028 Toulouse Cedex 4, France
[b] NASA Goddard Space Flight Center, Greenbelt, MD 20771, USA
[c] Space Sciences Laboratory, University of California, Berkeley, CA 94720, USA
[d] MPAe, Klatenburg – Lindau, Germany
[e] Bartol Research Institute, University of Delaware, Newark, DE 19716, USA
[f] NASA Jet Propulsion Laboratory, 4800 Oak Grove Drive, Pasadena, CA 91109, USA

Received 26 November 2002; received in revised form 19 March 2003; accepted 24 April 2003

Abstract

The magnetic pileup boundary (MPB) is a sharp, thin, and permanent plasma boundary reported, up to now, at comets and Mars, and located between the bow shock and the ionospheric boundary. The MPB separates the magnetosheath, a region with high wave activity, from the magnetic pileup region, where the interplanetary magnetic field piles up regularly in front of the planetary obstacle. We use magnetic field and electron plasma measurements from the MAG/ER experiment onboard the Mars Global Surveyor spacecraft to study two characteristic features of the MPB. The first feature is the sudden enhancement of the magnetic field line draping at the MPB. This new signature reveals that the MPB marks the entry into the veritable induced magnetosphere, where the magnetic field topology is more regular, in opposition to what is observed in the magnetosheath. Secondly, we study the properties and the occurrence of compressive, linearly polarized, low frequency waves, frequently observed on both sides of the boundary. An analysis of the correlation between the magnetic and the electron data reveals that on the upstream side the waves are mirror mode waves, while on the downstream side they are large amplitude, quasi-monochromatic fast magnetosonic waves. The presence of these features at other atmospheric, unmagnetized bodies can be used as indicators of the existence of a MPB.

Keywords: Solar wind interaction with unmagnetized bodies; Mars; MPB; Draping; Low frequency waves

1. Introduction

Since the arrival of the Mars Global Surveyor (MGS) spacecraft in September 1997, an enormous amount of plasma and magnetic field data has contributed to elucidate several key issues in the description of the Mars interaction with the solar wind. MGS measurements confirmed that this interaction is mainly of the atmospheric type due to the lack of a dynamo-generated global magnetic field, and the limited extent of the crustal magnetic field influence. One of the most notable features is the Magnetic Pileup Boundary (MPB) (Acuña et al., 1998), previously reported at comets (Neubauer, 1987; Mazelle et al., 1989, 1991, 1995). The MPB is a thin, sharp and permanent plasma boundary located between the bow shock and the ionospheric boundary. It separates the magnetosheath (MS), a region with high wave activity, from the inner magnetic pileup region (MPR) or magnetic barrier region (on the dayside), where the magnetic field is less disordered and more intense, as it piles up regularly in front of the planetary obstacle.

The MGS MAG/ER instrument consists of two redundant triaxial fluxgate magnetometers (MAG), and an electron reflectometer (ER) that measures the local electron distribution function between 10 eV and 20 keV

* Corresponding author. Present address: The Blackett Laboratory, Imperial College London, Prince Consort Road, London SW7 2BW, UK. Tel.: +44-207-594-7758.
E-mail address: c.bertucci@imperial.ac.uk (C. Bertucci).

0273-1177/$30 © 2004 COSPAR. Published by Elsevier Ltd. All rights reserved.
doi:10.1016/j.asr.2003.04.054

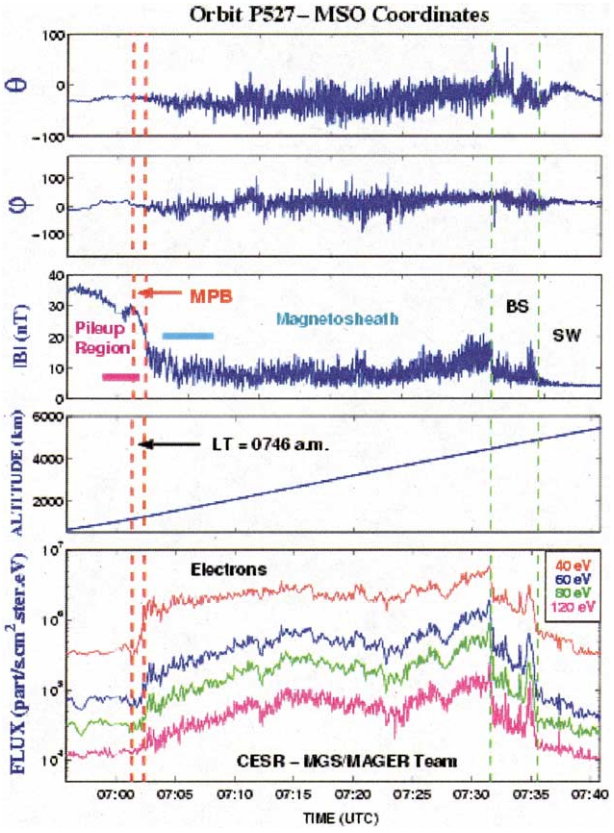

Fig. 1. The MPB as seen by MGS MAG/ER during a near terminator orbit. The MPB is crossed around 07:02 UTC, at 1200 km altitude and at 0746 am local time (Bertucci et al., 2003a).

(Acuña et al., 2001). Fig. 1 illustrates an example of a MPB crossing as seen by these instruments for an orbit near the terminator plane between 600 and 5430 km altitude. MAG data are given in Mars-centered Solar Orbital (MSO) coordinates. In this system, the x-axis points sunward, the y-axis is antiparallel to Mars' orbital velocity, and the z-axis completes the right-hand system. The three upper panels show the magnetic field vector in MSO spherical coordinates: θ is the elevation angle over Mars' orbital plane, ϕ is the azimuth (0° = sunward), and the magnetic field magnitude $|B|$. The lower panel shows the electron fluxes for four energy ranges labeled with their geometrical energy. Two boundaries are identified with two pairs of vertical dashed lines. First, the bow shock, crossed around 07:34 UTC. In the MS, the solar wind plasma continues to be decelerated and heated: the strong variability in the magnetic field direction and magnitude are followed by large fluctuations on the electron fluxes. The second boundary is the MPB and it is crossed around 07:02 UTC, at 1180 km altitude and at ~8 a.m. local time. The MPB is identified in the MGS MAG/ER data by three simultaneous features (Vignes et al., 2000): a jump in the magnetic field magnitude $|B|$ (which is generally sharp), a strong diminution of the variability of the magnetic field magnitude and orientation with respect to the MS, and a sharp decrease in the suprathermal electron fluxes associated to a cooling of the electron distribution function, as the cold electron density increases towards the planet (Grard et al., 1989). These observational signatures emerge in this example: $|B|$ goes from 10 nT up to 25–30 nT in less than 1 min (a ~100 km altitude range) and the suprathermal electron fluxes drop by nearly an order of magnitude. Since the MPB is a place where plasma properties change so drastically, changes in the plasma β and likely on anisotropies might also be expected. In the MPR, the magnetic field magnitude increases regularly and its orientation varies smoothly, as the ionospheric boundary (not shown here) is approached. In this study we analyze, from an observational point of view, two new characteristic signatures of the MPB associated to the aforementioned changes in the plasma properties. The first feature is related to the change in the magnetic field topology across the MPB, and the second one is the occurrence of low frequency, compressive waves at both sides of the boundary. Finally, we compare these results with similar studies at other atmospheric unmagnetized bodies.

2. Study of the magnetic field topology across the MPB

2.1. Method

Draping is one of the most distinctive features of the interaction of a highly conducting body with the magnetized solar wind. When the solar wind approaches such an obstacle carrying a field $\mathbf{B}_{\mathrm{IMF}}$ with a velocity $\mathbf{V}_{\mathrm{SW}}$, the field lines bend as if they were hung to the body on the dayside, while being stretched downstream as the flow passes the obstacle. The induced magnetosphere can be easily described using the (x_{IMF}, y_{IMF}, z_{IMF}) system

$$\hat{x}_{\mathrm{IMF}} = -\frac{\mathbf{V}_{\mathrm{SW}}}{|\mathbf{V}_{\mathrm{SW}}|}, \quad \hat{y}_{\mathrm{IMF}} = \frac{\mathbf{V}_{\mathrm{SW}} \times \mathbf{B}_{\mathrm{IMF}}}{|\mathbf{V}_{\mathrm{SW}} \times \mathbf{B}_{\mathrm{IMF}}|},$$

$$\hat{z}_{\mathrm{IMF}} = \hat{x}_{\mathrm{IMF}} \times \hat{y}_{\mathrm{IMF}}.$$

The magnetotail will be symmetric with respect to the (x_{IMF}, z_{IMF}) plane, with the current sheet lying on the (x_{IMF}, y_{IMF}) plane. Then, the projection of the magnetic field pattern on the (y_{IMF}, z_{IMF}) reminds that of a super conducting sphere embedded in a uniform magnetic field. The magnetic field line draping can be characterized from simple principles deduced from Fig. 2. First of all, we introduce a Mars-centered aberrated system, which takes into account the planet's orbital velocity on the solar wind direction. The aberrated (x', y', z') and the MSO (x, y, z) systems differ in a 4° – rotation around the z-axis. Fig. 2(a) shows the magnetic field projection on the (x_{IMF}, z_{IMF}) plane with the MGS trajectory. MGS crosses three different field lines at times t_a, t_b, t_c, ordered in function of decreasing altitude and $|x'|$ values. Because of draping, $|B_{x'}|$ increases from t_a to t_c.

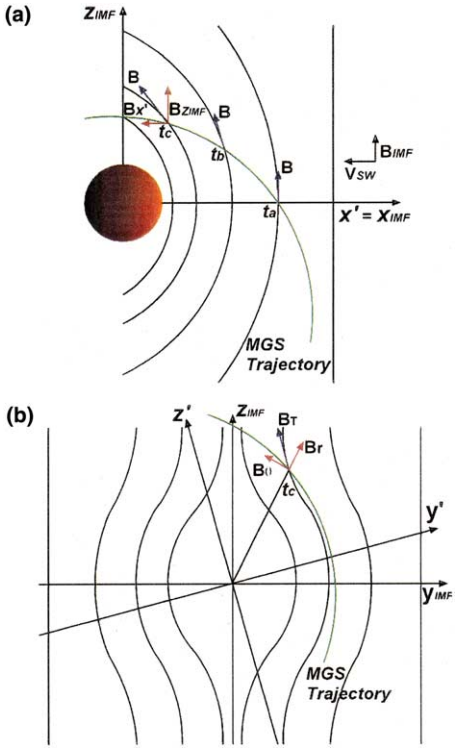

Fig. 2. (a) Draping geometry in the (x_{IMF}, z_{IMF}) plane, as MGS crosses 3 field lines at times t_a, t_b and t_c. $\mathbf{B}_{IMF}$ is normal to $\mathbf{V}_{SW}$ for clarity, (b). Slice perpendicular to $\mathbf{V}_{SW}$ field-pattern at t_c, and the projected MGS trajectory. The draping is revealed by the correlation between $B_{x'}$ and B_r (Bertucci et al., 2003a).

Simultaneously, the MGS positions at t_a, t_b and t_c define slices parallel to the (y_{IMF}, z_{IMF}) plane through the 3D field line structure. Fig. 2(b) shows only the slice at t_c with the IMF transverse component $\mathbf{B}_T$, its two cylindrical components B_r and B_θ, and the projected MGS trajectory. If several slices are considered, it can be easily demonstrated that in a draping regime the variation in $B_{x'}$ will be followed by a variation of $\mathbf{B}_T$ such that its radial cylindrical component B_r and $B_{x'}$ will be correlated, whether the spacecraft is in the inbound or the outbound leg. This result is valid as long as there are no discontinuities or strong fluctuations in the solar wind during the crossing of the interaction region. Thus, draping can be inferred regardless of the value of the IMF in the solar wind. This is especially important for MGS due to the uncertainty in the ambient magnetic field determination upstream from the bow shock (Acuña et al., 2001). In this study, we use calibrated, 0.75-s resolution data in the MS and in the MPR, where this effect is negligible.

2.2. Results

In classical single-fluid approaches (e.g. Liu et al., 2001), draping is expected to evolve progressively from the bow shock down to the ionopause. In such a sce-

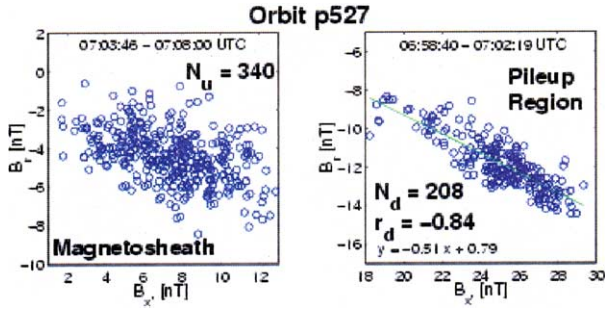

Fig. 3. $B_{x'}$ vs. B_r in the MS (left), and the MPR (right) for orbit p527. N_u and N_d are the number of points. On the right, the correlation coefficient r_d for the best linear least-square fit (Bertucci et al., 2003a).

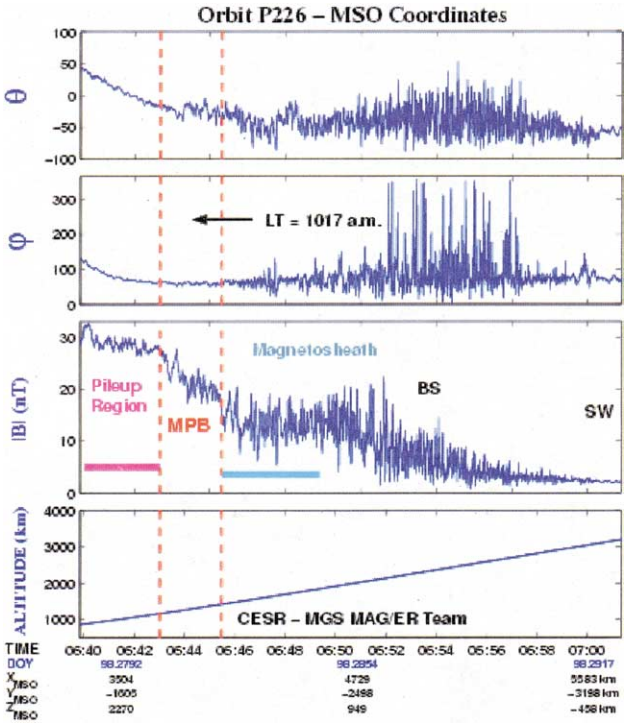

Fig. 4. Example of a MPB crossing for an orbit at ~10 a.m. local time (from Bertucci et al., 2003a).

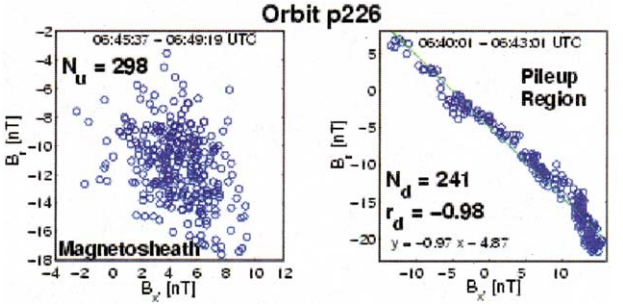

Fig. 5. $\mathbf{B}_{x'}$ vs. B_r in the MS and the MPR for orbit p226. N_u and N_d are the number of points. In the right panel, the correlation coefficient r_d for the best linear least-square fit is shown (Bertucci et al., 2003a).

Table 1
Linear correlation coefficients upstream (r_u) and downstream (r_d) from the Martian MPB

Orbit	LT_{MPB}	alt_{MPB} (km)	Δalt_u (km)	N_u	r_u	Δalt_d (km)	N_d	r_d
18	~5 p.m.	1277	1482–1927	71	−0.02	709–1010	58	0.96
122	~1 p.m.	728	999–1624	112	0.05	390–703	78	−0.95
226	~10 a.m.	1291	1441–1846	298	−0.38	883–1173	241	−0.98
527	~8 a.m.	1178	1372–1831	340	−0.45	867–1222	208	−0.84
1180	~3 p.m.	566	584–729	94	−0.31	500–578	51	−0.88

nario, a clear correlation between $B_{x'}$ and B_r should be expected anywhere between the bow shock and the obstacle. Fig. 3 summarizes the results of the correlation analysis between $B_{x'}$ and B_r for two intervals surrounding the MPB for the orbit described in Fig. 1 (horizontal segments in the $|B|$ panel). In the interval 07:03:46–07:08:00 UTC, just upstream from the MPB (left panel), the correlation is very poor indicating that draping is undetectable. In contrast, in the MPR (06:58:40–07:02:19 UTC), the very high linear correlation coefficient clearly reveals a sharp increase of the draping at the MPB (right panel). Fig. 4 shows another example. In this case, the MPB, crossed at ~10 a.m. local time and at 1300 km altitude, is identified from the signature on the suprathermal electron fluxes (not shown here) and from the decay in the fluctuations on θ and ϕ, but no drastic changes are observed in $|B|$. Again, two intervals adjacent to the MPB were analyzed (horizontal segments in the $|B|$ panel). For a comparable number of points, the difference between the correlation coefficients is even more significant (Fig. 5). The results for these and other MGS orbits are summarized in Table 1, including the spacecraft's local time (LT_{MPB}) and altitude (alt_{MPB}) at the MPB crossing, as well as the altitude range of the intervals upstream (Δalt_d) and downstream (Δalt_d) from the boundary. All types of MGS elliptical orbits were considered. The absolute value of the linear regression coefficients upstream from the MPB ($|r_u|$) remain below 0.5, while downstream from the MPB, $|r_d|$ remains above 0.8. For some orbits (e.g., p1180), crustal fields are observed near the periapsis, but the results show no significant difference with respect to crustal field free orbits.

3. Low frequency waves at the Martian MPB

3.1. Observations

The second feature is the occurrence of compressive, low frequency waves at both sides of the MPB. Fig. 6 shows MGS MAG/ER data for a ~10 a.m. local time orbit. The MPB is crossed a few seconds after 04:36 UTC, at ~700 km altitude. On both sides of the boundary, the magnetic field, steady in direction, displays high-amplitude fluctuations on the magnitude

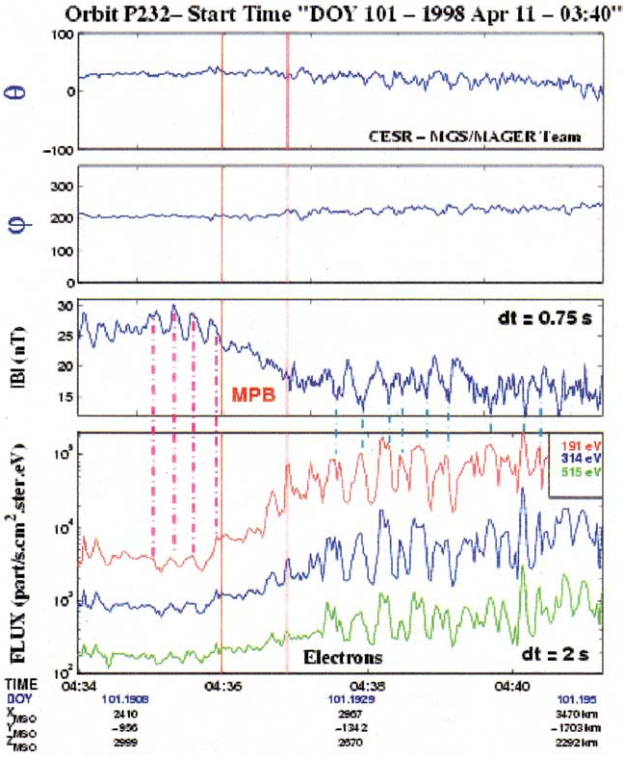

Fig. 6. MAG/ER data for ~10 a.m. local time orbit. Compressive, linearly-polarized low frequency waves can be observed at both sides of the MPB.

(compressive oscillations). The timescale of these fluctuations are of the order of a few tens of seconds (typically, 20 s), well below the local proton gyrofrequency at both sides of the boundary. On the upstream side, the oscillations in $|B|$ are "tooth shaped", i.e., a series of dips superimposed on a nearly constant background value. Inside the MPB, the waves are quasi-monochromatic and much more coherent. An analysis of the MAG data together with the ER data at both sides of the MPB is very useful in order to identify the modes to which these waves are associated. An examination of the suprathermal electron fluxes shows that there is an anticorrelation with $|B|$ upstream from the MPB, while downstream, the two quantities are correlated (vertical point-dash lines). In this figure, only the 190–520 eV range is depicted for clarity, but the same behavior is observed in all suprathermal energies.

3.2. Results

Fig. 7 displays MAG data in mean field coordinates for a typical example of wave event reported upstream from the MPB (type 1 waves). The computation of the mean field vector $\mathbf{B}_0$ from time average over the interval of the event permits to separate the magnetic field component along this direction ($B_{//}$), from the components on the normal plane (B_{perp1} and B_{perp2}). The parallel component is the only that reproduces the oscillations, while the other two have very marginal values, revealing that the wave is linearly polarized along B_0. Finally, minimum variance analysis (MVA) helps to show that the $\mathbf{k}$ vector is nearly perpendicular to $\mathbf{B}_0$ ($\theta_{\mathrm{KB}} = 89°$). The events reported downstream from the MPB (type 2 waves) can be analyzed in a similar way. Fig. 8 shows the magnetic field components in the direction $\mathbf{k} \times \mathbf{B}_0$ and $\mathbf{k} \times (\mathbf{k} \times \mathbf{B}_0)$, where $\mathbf{k}$ is calculated from MVA and $\mathbf{B}_0$ is estimated as before. The oscillation is fully reproduced in the $\mathbf{k} \times (\mathbf{k} \times \mathbf{B}_0)$ component, indicating that these waves are also compressive and linearly polarized, with a wave vector normal to $\mathbf{B}_0(\theta_{\mathrm{KB}} = 88°)$. A survey of 282 MPB crossings by MGS shows that type 1 waves occur in at least 48%, type 2 waves in at least 27%, and both modes simultaneously in at least 18% of the observations. Finally, at least 11% of the observations show neither type 1 nor type 2 waves.

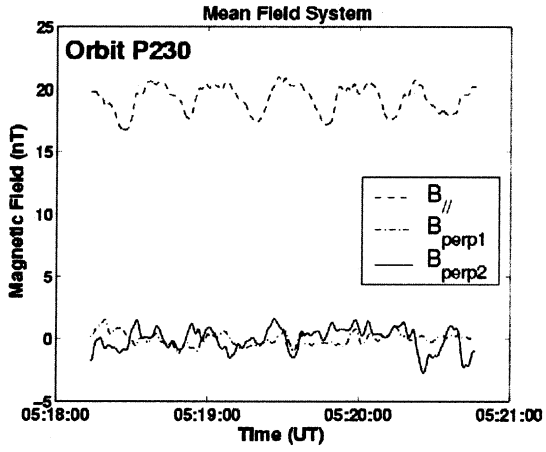

Fig. 7. MAG data in Mean Field coordinates during a wave event reported just upstream from the MPB (for more details see text).

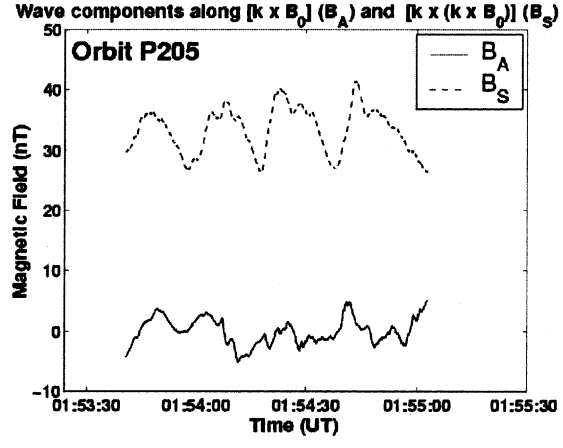

Fig. 8. Magnetic field along $\mathbf{k} \times \mathbf{B}_0$, and $\mathbf{k} \times (\mathbf{k} \times \mathbf{B}_0)$, ($B_{\mathrm{A}}$ and B_{S}, respectively), for a wave event downstream from the MPB (for more details see text).

4. Discussion

The results confirm a strong and sudden enhancement of the magnetic field draping at the MPB of Mars, in contrast with the picture of a gradual draping between the bow shock and the final planetary obstacle. In opposition to what happens in the MS, the magnetic field becomes suddenly organized as the MPB is crossed. The boundary marks then the entrance into a veritable induced magnetosphere., where draping is strong (Bertucci et al., 2003a). In this region, the magnetic field lines frozen in the electrons follow a denser and cooler plasma. This is a consequence of the mass loading and ionization mechanisms (electron impact and charge exchange) which contribute to the dominance of heavy ions of exospheric origin (Lundin et al., 1990; Crider et al., 2000). The lower limit of this region is the final planetary obstacle, disregarding of its nature (Luhmann, 1986; Mitchell et al., 2001). These results are highly consistent with Phobos 2 observations across the magnetic tail boundary at 2.86 R_{M}(Yeroshenko et al., 1990). Israelevich et al. (1994) obtained the same result when applying this method on Giotto spacecraft magnetometer data at comet P/Halley. Similar properties have been observed at comet P/Grigg–Skjellerup MPB (Neubauer et al., 1993), and across comet P/Giacobini–Zinner (G–Z) magnetotail by ICE. Slavin et al. (1986) report turbulent, weakly-draped magnetic fields in the magnetosheath of G–Z, while in the magnetotail, the field is stronger and adopts a draped configuration. This confirms that not only at comets (Neubauer, 1987), but also at Mars, the MPB is the dayside counterpart and the origin of the tail boundary.

The enhancement of the draping has been observed in numerous MGS orbits regardless of the presence of crustal magnetic sources and the strength of the gradient in $|B|$ at the MPB. The latter conclusion led Bertucci et al. (2002) to do an identical study on Pioneer Venus magnetometer data in the external part of the magnetic barrier region of Venus (Zhang et al., 1991), where a weak gradient is frequently observed. As a result, they report a sudden and strong enhancement of the draping across a very thin layer or boundary at the entrance into the magnetic barrier region on the dayside (well above the ionopause) regardless of the presence of a strong jump in the magnetic field magnitude. More recently,

Bertucci et al., 2003b) conclude that this "draping boundary" represents in fact the Venusian equivalent of the MPB and the dayside counterpart of the Venusian tail boundary. This conclusion is compatible with the results of a study on the magnetic tail boundary (the surface separating highly draped fields from the less organized magnetosheath fields) by Saunders and Russell (1986), who affirm that the magnetic field lines in the nightside that cross this boundary should close on the dayside well above the ionopause. As for Venus, the gradual $|B|$ profile in Vega 1 and 2 magnetic field data when entering into comet P/Halley MPR did not permit the identification of the MPB. Nevertheless, Bertucci et al. (2002) show that analyses of the three-dimensional field topology like this one between the MS and the MPR provide key information to locate the boundary.

Single-fluid models have difficulties reproducing such a localized enhancement of draping since no limit constraint other than the impenetrable inner boundary can be introduced. Hybrid and 2-ion fluid (e.g., Sauer and Dubinin, 2000) approaches could be used in an attempt to reproduce and interpret such a striking feature.

The occurrence of compressive, low frequency waves is another characteristic feature of the Martian MPB. The characteristics of the waves upstream from the boundary (linearly polarized, quasi-perpendicular propagation, anti-correlation between $|B|$ and the suprathermal electron density) are those of mirror mode waves. This purely kinetic mode is stationary in the plasma frame ($\omega_r = 0$) for a homogeneous medium. It is driven by anisotropies in the plasma pressure ($\beta_\perp/\beta_{//} > 1 + 1/\beta_\perp$, where β is the ratio of plasma to magnetic pressure), especially when β is high. At Mars these waves have lengthscales of several upstream proton gyroradii, which is consistent with theoretical properties. One of the possible sources for generating anisotropies is the heating of the ion population downstream from quasi-perpendicular shocks, as at the Earth (e.g., Lacombe et al., 1995). Interestingly, mirror mode waves at Mars occur whatever the shock's nature, and they always appear to be "attached" to the MPB, as if they were convected down to it. Distributions (likely non-gyrotropic) of newborn pickup ions (especially heavies, e.g. O^+) also provide large $\beta_\perp$ values upstream from the MPB. In the case of comets, mirror-mode waves were reported on the outer side of the magnetic tail boundary of P/Giacobini–Zinner (Tsurutani et al., 1999). This is another evidence in favor of the connection between the MPB and the magnetic tail boundary. The properties of the waves downstream from the MPB coincide with those of magnetosonic fast-mode waves. It is difficult to account for the properties of such waves from locally growing plasma microinstabilities (especially perpendicular propagation), in light of their large amplitude and the small scale of the MPR. Such waves could be interpreted as stationary, bi-ion waves standing downstream from the MPB (Sauer et al., 1989). The same correspondence mirror/fast magnetosonic mode was reported by Mazelle et al. (1991) at both sides of comet P/Halley MPB. Glassmeier et al. (1993) suggest an equivalent interpretation for the waves downstream from the MPB, but further study is needed in this respect. At Venus, the magnetosheath is a region with relatively high plasma beta, in opposition to MPR where the plasma beta is low. Accordingly, we might expect different wave modes in each region. However, the plasma temperature anisotropy and the $|B|$ values in the Venusian magnetosheath are such that the instability threshold for mirror modes is not necessarily reached. In any case, a survey of ultra low frequency waves near the outer edge of the MPR should be done using PVO magnetometer data in order to investigate if this frequent but not permanent wave feature observed at Mars and comets occurs also at Venus.

The MPB is also a boundary for higher frequency waves. Despite the lack of wave instruments onboard MGS, a significant amount of information on higher frequency waves was obtained by the Plasma Wave System (PWS) onboard PHOBOS-2 in the same region. Trotignon et al. (1996) report from PWS data the presence of a boundary, the so-called "planetopause". It is characterized by a decrease in the spacecraft potential indicating an increase in the plasma pressure, a peak in the electric field level between dc up to 6 kHz, a local minimum in the plasma turbulence and, an increase in the total electron plasma density deduced from the enhancement in the Langmuir probe current fluctuation. Then, the authors calculated the boundary mean position and shape by fitting a conic section from 37 crossings. In 2000, Vignes et al. fitted a conic section on 488 MPB crossings identified using MGS MAG/ER data and concluded that the "planetopause" and the MPB are the same plasma boundary.

In summary, the presence of these two features at the MPB of Mars and comets and the presence of at least one of them at Venus strengthen the idea that these are common characteristics for all atmospheric/exospheric interaction-type bodies with the solar wind, as well as good indicators of the presence of the MPB.

References

Acuña, M.H., Connerney, J.E.P., Wasilewski, P., et al. Magnetic field and plasma observations at Mars: initial results of the Mars Global Surveyor Mission. Science 279, 1676–1680, 1998.

Acuña, M.H., Connerney, J.E.P., Wasilewski, P., et al. Magnetic field of Mars: summary of results from the aero-braking and mapping orbits. J. Geophys. Res. 106 (E10), 23,403–23,418, 2001.

Bertucci, C., Mazelle, C., Crider, D.H., et al. Magnetic Field Draping Enhancement at Weakly Magnetized Bodies. Eos Trans. AGU, 53(47), Fall Meet. Suppl., Abstract P21B-0380, 2002.

Bertucci, C., Mazelle, C., Crider, D.H., et al. Magnetic field draping enhancement at the Martian magnetic pileup boundary from Mars

Global Surveyor observations. Geophys. Res. Lett. 30 (2), 1099, 2003a, doi: 10.1029/2002GL015713.

Bertucci, C., Mazelle, C., Slavin, J.A., et al. Magnetic field draping enhancement at Venus: evidence for a magnetic pileup boundary. Geophys. Res. Lett. 30(17), SSC1–1, CiteID 1876, doi:10.1029/2003GL017271, 2003b.

Crider, D., Cloutier, P., Law, C., et al. Evidence of electron impact ionization in the magnetic pileup boundary of Mars. Geophys. Res. Lett. 27 (1), 45, 2000.

Glassmeier, K.H., Motschmann, U., Mazelle, C., et al. Mirror modes and fast magnetoacoustic waves near the magnetic pileup boundary of comet P/Halley. J. Geophys. Res. A 12, 20955–20964, 1993.

Grard, R.A., Pedersen, A., Klimov, S., et al. First measurements of plasma waves near Mars. Nature 341, 607–609, 1989.

Israelevich, P.L., Neubauer, F.M., Ershkovich, A. The induced magnetosphere of comet Halley: interplanetary magnetic field during Giotto encounter. J. Geophys. Res. 99 (A4), 6575–6583, 1994.

Lacombe, C., Belmont, G., Hubert, D., et al. Density and magnetic field fluctuations observed by ISEE 1-2 in the quiet magnetosheath. Ann. Geophysicae 13, 343–357, 1995.

Liu, Y., Nagy, A.F., Gombosi, T.I., et al. The solar wind interaction with Mars: results of three-dimensional three-species MHD studies. Adv. Space Res. 27 (11), 1837–1846, 2001.

Luhmann, J.G. The solar wind interaction with Venus. Space Sci. Rev. 44, 241–306, 1986.

Lundin, R., Zakharov, A., Pellinen, R., et al. Plasma composition measurements of the Martian magnetosphere morphology. Geophys. Res. Lett. 17 (6), 877–880, 1990.

Mazelle, C., Rème, H., Sauvaud, J.A., et al. Analysis of suprathermal electron properties at the magnetic pile-up boundary of comet P/Halley. Geophys. Res. Lett. 16 (9), 1035–1038, 1989.

Mazelle, C., Rème, H., Belmont, G., et al. Ultra low frequency waves at the magnetic pile-up boundary of comet P/Halley. Adv. Space Res. 11 (9), 73–77, 1991.

Mazelle, C., Rème, H., Neubauer, F.M., et al. Comparison of the main magnetic and plasma features in the environments of comets Grigg–Skjellerup and Halley. Adv. Space Res. 16 (4), 41–45, 1995.

Mitchell, D.L., Lin, R.P., Mazelle, C., et al. Probing Mars' crustal magnetic field and ionosphere with the MGS Electron Reflectometer. J. Geophys. Res. 106 (E10), 23419–23427, 2001.

Neubauer, F.M. Giotto magnetic-field results on the boundaries of the pile-up region and the magnetic cavity. Astron. Astrophys. 187, 73–79, 1987.

Neubauer, F.M., Marschall, H., Pohl, M., et al. First results from the Giotto magnetometer experiment during the P/Grigg-Skjellerup encounter. Astron. Astrophys. 268, L5–L8, 1993.

Sauer, K., Motschmann, U., Baumgärtel, K. Multifluid simulations of the solar wind–comet interaction. Adv. Space Res. 9, 309–312, 1989.

Sauer, K., Dubinin, E. The nature of the Martian 'Obstacle Boundary'. Adv. Space Res. 26 (10), 1633–1637, 2000.

Saunders, M.A., Russell, C.T. Average dimension and magnetic structure of the distant Venus magnetotail. J. Geophys. Res. 95 (A5), 5589–5604, 1986.

Slavin, J.A., Smith, E.J., Tsurutani, B.T., et al. Giacobini–Zinner magnetotail – ice magnetic field observations. Geophys. Res. Lett. 13 (3), 283–286, 1986.

Trotignon, J.-G., Dubinin, E., Grard, R., et al. Martian planetopause as seen by the plasma wave system onboard Phobos 2. J. Geophys. Res. 101 (A11), 24965–24977, 1996.

Tsurutani, B., Lakhina, G.S., Smith, E.J., et al. Mirror mode structures and ELF plasma waves in the Giacobini–Zinner magnetosheath. Nonlinear Proc. Geophys. 6, 229–234, 1999.

Vignes, D., Mazelle, C., Rème, H., et al. The solar wind interaction with Mars: locations and shapes of the Bow Shock and the Magnetic pile-up boundary from the observations of the MAG/ER experiment onboard Mars Global Surveyor. Geophys. Res. Lett. 27 (1), 49–52, 2000.

Yeroshenko, Y., Riedler, W., Scwingenschuh, K., et al. The magnetotail of Mars: Phobos observations. Geophys. Res. Lett. 17 (6), 885–888, 1990.

Zhang, T., Luhmann, J.G., Russell, C.T. The magnetic barrier at Venus. J. Geophys. Res. 96 (A7), 1145–11153, 1991.